Full vectorial analysis of polarization effects in optical nanowires

Shahraam Afshar V.*, M. A. Lohe, Wen Qi Zhang, and Tanya M. Monro

Institute for Photonics & Advanced Sensing (IPAS), The University of Adelaide, 5005, Australia

**shahraam.afshar@adelaide.edu.au*

Abstract: We develop a full theoretical analysis of the nonlinear interactions of the two polarizations of a waveguide by means of a vectorial model of pulse propagation which applies to high index subwavelength waveguides. In such waveguides there is an anisotropy in the nonlinear behavior of the two polarizations that originates entirely from the waveguide structure, and leads to switching properties. We determine the stability properties of the steady state solutions by means of a Lagrangian formulation. We find all static solutions of the nonlinear system, including those that are periodic with respect to the optical fiber length as well as nonperiodic soliton solutions, and analyze these solutions by means of a Hamiltonian formulation. We discuss in particular the switching solutions which lie near the unstable steady states, since they lead to self-polarization flipping which can in principle be employed to construct fast optical switches and optical logic gates.

OCIS codes: (190.4360) Nonlinear optics, devices; (190.4370) Nonlinear optics, fibers; (190.3270) Kerr effect; (130.4310) Integrated optics (nonlinear); (060.4005) Microstructured fibers; (060.5530) Pulse propagation and temporal solitons.

References and links

1. R. H. Stolen, J. Botineau, and A. Ashkin, "Intensity discrimination of optical pulses with birefringent fibers," Opt. Lett. **7**, 512–514 (1982).
2. F. Matera and S. Wabnitz, "Nonlinear polarization evolution and instability in a twisted birefringent fiber," Opt. Lett. **11**, 467–469 (1986).
3. H. G. Winful, "Polarization instabilities in birefringent nonlinear media: application to fiber-optic devices," Opt. Lett. **11**, 33–35 (1986).
4. C. Menyuk, "Nonlinear pulse propagation in birefringent optical fibers," IEEE J. Quantum Electron. **23**, 174–176 (1987).
5. S. F. Feldman, D. A. Weinberger, and H. G. Winful, "Polarization instability in a twisted birefringent optical fiber," J. Opt. Soc. Am. B **10**, 1191–1201 (1993).
6. G. Millot, E. Seve, and S. Wabnitz, "Polarization symmetry breaking and pulse train generation from the modulation of light waves," Phys. Rev. Lett. **79**, 661–664 (1997).
7. G. Millot, E. Seve, S. Wabnitz, and M. Haelterman, "Dark-soliton-like pulse-train generation from induced modulational polarization instability in a birefringent fiber," Opt. Lett. **23**, 511–513 (1998).
8. S. Pitois, G. Millot, and S. Wabnitz, "Polarization domain wall solitons with counterpropagating laser beams," Phys. Rev. Lett. **81**, 1409–1412 (1998).
9. S. Pitois, G. Millot, and S. Wabnitz, "Nonlinear polarization dynamics of counterpropagating waves in an isotropic optical fiber: theory and experiments," J. Opt. Soc. Am. B **18**, 432–443 (2001).
10. S. Wabnitz, "Polarization domain wall solitons in elliptically birefringent optical fibers," PIERS ONLINE **5**, 621–624 (2009).

#165808 - $15.00 USD Received 30 Mar 2012; revised 27 May 2012; accepted 30 May 2012; published 14 Jun 2012

11. V. V. Kozlov and S. Wabnitz, "Theoretical study of polarization attraction in high-birefringence and spun fibers," Opt. Lett. **35**, 3949–3951 (2010).
12. J. Fatome, S. Pitois, P. Morin, and G. Millot, "Observation of light-by-light polarization control and stabilization in optical fibre for telecommunication applications," Opt. Express **18**, 15311–15317 (2010).
13. V. V. Kozlov, J. Nuño, and S. Wabnitz, "Theory of lossless polarization attraction in telecommunication fibers," J. Opt. Soc. Am. B **28**, 100–108 (2011).
14. V. E. Zakharov and A. V. Mikhailov, "Polarization domains in nonlinear optics," JETP Lett. **45**, 349–352 (1987).
15. S. Pitois, A. Picozzi, G. Millot, H. R. Jauslin, and M. Haelterman, "Polarization and modal attractors in conservative counterpropagating four-wave interaction," Europhys. Lett. **70**, 88–94 (2005).
16. S. Pitois, J. Fatome, and G. Millot, "Polarization attraction using counter-propagating waves in optical fiber at telecommunication wavelengths," Opt. Express **16**, 6646–6651 (2008).
17. S. Wabnitz, "Cross-polarization modulation domain wall solitons for WDM signals in birefringent optical fibers," IEEE Photon. Technol. Lett. **21**, 875–877 (2009).
18. E. Seve, G. Millot, S. Trillo, and S. Wabnitz, "Large-signal enhanced frequency conversion in birefringent optical fibers: theory and experiments," J. Opt. Soc. Am. B **15**, 2537–2551 (1998).
19. G. Gregori and S. Wabnitz, "New exact solutions and bifurcations in the spatial distribution of polarization in third-order nonlinear optical interactions," Phys. Rev. Lett. **56**, 600–603 (1986).
20. S. M. Jensen, "The nonlinear coherent coupler," IEEE J. Quantum Electron. **18**, 1580–1583 (1982).
21. C. M. de Sterke and J. E. Sipe, "Polarization instability in a waveguide geometry," Opt. Lett. **16**, 202–204 (1991).
22. Y. Wang and W. Wang, "Nonlinear optical pulse coupling dynamics," J. Lightwave Technol. **24**, 2458–2464 (2006).
23. Y. S. Kivshar, "Switching dynamics of solitons in fiber directional couplers," Opt. Lett. **18**, 7–9 (1993).
24. D. C. Hutchings, J. S. Aitchison, and J. M. Arnold, "Nonlinear refractive coupling and vector solitons in anisotropic cubic media," J. Opt. Soc. Am. B **14**, 869–879 (1997).
25. H. S. Eisenberg, Y. Silberberg, R. Morandotti, A. R. Boyd, and J. S. Aitchison, "Discrete spatial optical solitons in waveguide arrays," Phys. Rev. Lett. **81**, 3383–3386 (1998).
26. U. Peschel, R. Morandotti, J. M. Arnold, J. S. Aitchison, H. S. Eisenberg, Y. Silberberg, T. Pertsch, and F. Lederer, "Optical discrete solitons in waveguide arrays. 2. dynamic properties," J. Opt. Soc. Am. B **19**, 2637–2644 (2002).
27. K. R. Khan, T. X. Wu, D. N. Christodoulides, and G. I. Stegeman, "Soliton switching and multi-frequency generation in a nonlinear photonic crystal fiber coupler," Opt. Express **16**, 9417–9428 (2008).
28. C. C. Yang, "All-optical ultrafast logic gates that use asymmetric nonlinear directional couplers," Opt. Lett. **16**, 1641–1643 (1991).
29. T. Fujisawa and M. Koshiba, "All-optical logic gates based on nonlinear slot-waveguide couplers," J. Opt. Soc. Am. B **23**, 684–691 (2006).
30. W. Fraga, J. Menezes, M. da Silva, C. Sobrinho, and A. Sombra, "All optical logic gates based on an asymmetric nonlinear directional coupler," Opt. Commun. **262**, 32–37 (2006).
31. D. C. Hutchings and B. S. Wherrett, "Theory of the anisotropy of ultrafast nonlinear refraction in zinc-blende semiconductors," Phys. Rev. B **52**, 8150–8159 (1995).
32. G. P. Agrawal, *Nonlinear Fiber Optics* (Academic Press, 2007).
33. S. Afshar V. and T. M. Monro, "A full vectorial model for pulse propagation in emerging waveguides with subwavelength structures part I: Kerr nonlinearity," Opt. Express **17**, 2298–2318 (2009).
34. J. B. Driscoll, X. Liu, S. Yasseri, I. Hsieh, J. I. Dadap, and R. M. Osgood, "Large longitudinal electric fields (E_z) in silicon nanowire waveguides," Opt. Express **17**, 2797–2804 (2009).
35. B. A. Daniel and G. P. Agrawal, "Vectorial nonlinear propagation in silicon nanowire waveguides: polarization effects," J. Opt. Soc. Am. B **27**, 956–965 (2010).
36. V. R. Almeida, Q. Xu, C. A. Barrios, and M. Lipson, "Guiding and confining light in void nanostructure," Opt. Lett. **29**, 1209–1211 (2004).
37. O. Boyraz, P. Koonath, V. Raghunathan, and B. Jalali, "All optical switching and continuum generation in silicon waveguides," Opt. Express **12**, 4094–4102 (2004).
38. C. Koos, P. Vorreau, T. Vallaitis, P. Dumon, W. Bogaerts, R. Baets, B. Esembeson, I. Biaggio, T. Michinobu, F. Diederich, W. Freude, and J. Leuthold, "All-optical high-speed signal processing with silicon-organic hybrid slot waveguides," Nat. Photon. **3**, 216–219 (2009).
39. W. Astar, J. B. Driscoll, X. Liu, J. I. Dadap, W. M. J. Green, Y. A. Vlasov, G. M. Carter, and R. M. Osgood, "Tunable wavelength conversion by XPM in a silicon nanowire, and the potential for XPM-multicasting," J. Lightwave Technol. **28**, 2499–2511 (2010).
40. R. K. W. Lau, M. Ménard, Y. Okawachi, M. A. Foster, A. C. Turner-Foster, R. Salem, M. Lipson, and A. L. Gaeta, "Continuous-wave mid-infrared frequency conversion in silicon nanowaveguides," Opt. Lett. **36**, 1263–1265 (2011).
41. M. Pelusi, F. Luan, T. D. Vo, M. R. E. Lamont, S. J. Madden, D. A. Bulla, D.-Y. Choi, B. Luther-Davis, and B. J. Eggleton, "Photonic-chip-based radio-frequency spectrum analyser with terahertz bandwidth," Nat. Photon. **3**, 139–143 (2009).
42. X. Gai, T. Han, A. Prasad, S. Madden, D.-Y. Choi, R. Wang, D. Bulla, and B. Luther-Davies, "Progress in optical

#165808 - $15.00 USD Received 30 Mar 2012; revised 27 May 2012; accepted 30 May 2012; published 14 Jun 2012

waveguides fabricated from chalcogenide glasses," Opt. Express **18**, 26635–26646 (2010).
43. B. J. Eggleton, B. Luther-Davies, and K. Richardson, "Chalcogenide photonics," Nat. Photon. **5**, 141–148 (2011).
44. P. Petropoulos, T. M. Monro, W. Belardi, K. Furusawa, J. H. Lee, and D. J. Richardson, "2R-regenerative all-optical switch based on a highly nonlinear holey fiber," Opt. Lett. **26**, 1233–1235 (2001).
45. H. Ebendorff-Heidepriem, P. Petropoulos, S. Asimakis, V. Finazzi, R. C. Moore, K. Frampton, F. Koizumi, D. J. Richardson, and T. M. Monro, "Bismuth glass holey fibers with high nonlinearity," Opt. Express **12**, 5082–5087 (2004).
46. S. Afshar V., W. Q. Zhang, H. Ebendorff-Heidepriem, and T. M. Monro, "Small core optical waveguides are more nonlinear than expected: experimental confirmation," Opt. Lett. **34**, 3577–3579 (2009).
47. G. Qin, X. Yan, C. Kito, M. Liao, T. Suzuki, A. Mori, and Y. Ohishi, "Highly nonlinear tellurite microstructured fibers for broadband wavelength conversion and flattened supercontinuum generation," J. Appl. Phys. **107**, 043108 (2010).
48. F. Poletti, X. Feng, G. M. Ponzo, M. N. Petrovich, W. H. Loh, and D. J. Richardson, "All-solid highly nonlinear singlemode fibers with a tailored dispersion profile," Opt. Express **19**, 66–80 (2011).
49. M. D. Turner, T. M. Monro, and S. Afshar V., "A full vectorial model for pulse propagation in emerging waveguides with subwavelength structures part II: Stimulated Raman scattering," Opt. Express **17**, 11565–11581 (2009).
50. W. Q. Zhang, M. A. Lohe, T. M. Monro, and S. Afshar V., "Nonlinear polarization bistability in optical nanowires," Opt. Lett. **36**, 588–590 (2011).
51. S. Afshar V., W. Q. Zhang, and T. M. Monro, "Structurally-based nonlinear birefringence in waveguides with subwavelength structures and high index materials," in "ACOFT 2009 Proceeding," (Australian Optical Society, 2009), 374–375.
52. E. Mägi, L. Fu, H. Nguyen, M. Lamont, D. Yeom, and B. Eggleton, "Enhanced Kerr nonlinearity in sub-wavelength diameter As_2Se_3 chalcogenide fiber tapers," Opt. Express **15**, 10324–10329 (2007).
53. S. Coleman, "Classical lumps and their quantum descendents," in *New Phenomena in Subnuclear Physics* Ed. A. Zichichi (New York, 1977), 185–264.
54. Y. S. Kivshar and G. P. Agrawal, *Optical Solitons: from Fibers to Photonic Crystals* (Academic Press, 2003)
55. W. Q. Zhang, M. A. Lohe, T. M. Monro, and S. Afshar V., "Nonlinear self-flipping of polarization states in asymmetric waveguides," arXiv:1203.6416
56. W. Q. Zhang, M. A. Lohe, T. M. Monro, and S. Afshar V., "Nonlinear polarization self-flipping and optical switching," in Proceedings of the International Quantum Electronics Conference and Conference on Lasers and Electro-Optics Pacific Rim 2011, (Optical Society of America, 2011), paper C370.
57. I. S. Gradshteyn and I. M. Ryzhik, *Table of Integrals, Series and Products* (Academic Press, 1965).
58. W. Q. Zhang, M. A. Lohe, T. M. Monro, and S. Afshar V., "New regimes of polarization bistability in linear birefringent waveguides and optical logic gates," in Nonlinear Photonics, OSA Technical Digest (CD) (Optical Society of America, 2010), paper NThD4.

1. Introduction

The Kerr nonlinear interaction of the two polarizations of the propagating modes of a waveguide leads to a host of physical effects that are significant from both fundamental and application points of view. Here, we develop a model of nonlinear interactions of the two polarizations using full vectorial nonlinear pulse propagation equations, with which we analyze the nonlinear interactions in the emerging class of subwavelength and high index optical waveguides. Based on this model we predict an anisotropy that originates solely from the waveguide structure, and which leads to switching states that can in principal be used to construct optical devices such as switches or logical gates. We derive the underlying nonlinear Schrödinger equations of the vectorial model with explicit integral expressions for the nonlinear coefficients. We analyze solutions of these nonlinear pulse propagation equations and the associated switching states by means of a Lagrangian formulation, which enables us to determine stability properties of the steady states; this formulation provides a global view of all solutions and their properties by means of the potential function and leads, for example, to the emergence of kink solitons as solutions to the model equations. We also use a Hamiltonian formalism in order to identify periodic and solitonic trajectories, including solutions that allow polarization flipping, and find conditions under which the unstable states and associated switching solutions are experimentally accessible. In order to provide examples of parameter values for which the predicted behavior occurs, we perform numerical calculations for waveguides with elliptical cross sec-

#165808 - $15.00 USD Received 30 Mar 2012; revised 27 May 2012; accepted 30 May 2012; published 14 Jun 2012

tions, although the underlying model is applicable to arbitrary fiber geometries.

The nonlinear interactions of the two polarizations of the propagating modes of a waveguide have been studied extensively over the last 30 years [1–13]. Different aspects of the interactions have been investigated, for example Stolen et al. [1] used the induced nonlinear phase difference between the two polarizations to discriminate between high and low power pulses. In the context of counterpropagating waves, the nonlinear interactions have been shown to lead to polarization domain wall solitons, [8–10] which are described as kink solitons representing a polarization switching between different domains with orthogonal polarization states. The nonlinear interactions can also lead to polarization attraction [9, 11–13, 15, 16] where the state of the polarization of a signal is attracted towards that of a pump beam. For twisted birefringent optical fibers, polarization instability [2, 5] and polarization domain wall solitons [17] have been reported. The nonlinear interactions also induce modulation instability which results in dark-soliton-like pulse-train generation [6, 7]. Large-signal enhanced frequency conversion [18], cross-polarization modulation for WDM signals [10], and polarization instability [3] have also been reported and attributed to nonlinear polarization interactions. Stability behavior has been studied in anisotropic crystals [19].

The nonlinear interactions of the two polarizations can also be studied in the context of either *nonlinear coherent coupling* or *nonlinear directional coupling* in which the amplitudes of two or more electric fields, either the two polarizations of a propagating mode of a waveguide or different modes of different waveguides, couple to each other through linear and nonlinear effects [20–22]. Nonlinear directional coupling is relevant to ultrafast all-optical switching, such as soliton switching [23–27] and all-optical logic gates [28–30]. The interaction of ultrafast beams, with different frequencies and polarizations, in anisotropic media has also been studied and the conditions for polarization stability have been identified [24, 31].

In previous work ([32], Chapter 6), the nonlinear interactions of the two polarizations are described by two coupled Schrödinger equations. These equations employ the weak guidance approximation, which assumes that the propagating modes of the two polarizations of the waveguide are purely transverse and orthogonal to each other within the transverse x,y plane, perpendicular to the direction of propagation z. Based on this, the electric fields are written as

$$\mathbf{E}_i(x,y,z,t) = A_i(z,t)\mathbf{e}_i(x,y), \quad i = 1,2, \tag{1}$$

where $A_i(z,t)$ are the amplitudes of the two polarizations, with $\mathbf{e}_1(x,y)\,.\,\mathbf{e}_2(x,y) = e_1(x,y)e_2(x,y)\hat{\mathbf{x}}\,.\,\hat{\mathbf{y}} = 0$, where $e_1(x,y), e_2(x,y)$ are the transverse distributions of the two polarizations, $\hat{\mathbf{x}}, \hat{\mathbf{y}}$ are unit vectors along the x and y directions, and it is understood that fast oscillatory terms of the form $\exp(-i\omega t \pm \beta_i z)$ are to be included for the polarization fields. The weak guidance approximation also assumes that the Kerr nonlinear coefficients for the self phase modulation of the two polarizations are equal because their corresponding mode effective areas are equal [32]. We refer here to models of nonlinear pulse propagation based on the weak guidance approximation simply as "scalar" models, since these models consider only purely transverse modes for the two polarizations.

The weak guidance approximation works well only for waveguides with low index contrast materials, and large dimension structure compared to the operating wavelength. This approximation is, however, no longer appropriate for high index contrast subwavelength scale waveguides (HIS-WGs) [33–35]. These waveguides have recently attracted significant interest mainly due to their extreme nonlinearity and possible applications for all optical photonic-chip devices. Examples include silicon, chalcogenide, or soft glass optical waveguides, which have formed the base for three active field of studies: silicon photonics [36–40], chalcogenide photonics [41–43], and soft glass microstructured photonic devices [44–48].

In order to address the limitations of the scalar models in describing nonlinear processes in HIS-WGs, we have developed in [33] a full vectorial nonlinear pulse propagation model.

#165808 - $15.00 USD Received 30 Mar 2012; revised 27 May 2012; accepted 30 May 2012; published 14 Jun 2012

Important features of this model are: (1) the propagating modes of the waveguide are not, in general, transverse and have large z components and, (2) the orthogonality condition of different polarizations over the cross section of the waveguide is given by $\int \mathbf{e}_1(x,y) \times \mathbf{h}_2^*(x,y) \cdot \hat{\mathbf{z}}\, \mathrm{d}A = 0$, rather than simply $\mathbf{e}_1(x,y) \cdot \mathbf{e}_2(x,y) = 0$ as in the scalar models. These aspects lead to an improved understanding of many nonlinear effects in HIS-WGs; it was predicted in [33], for example, that within the vectorial model the Kerr effective nonlinear coefficients of HIS-WGs have higher values than those predicted by the scalar models due to the contribution of the z-component of the electric field, as later confirmed experimentally [46]. Similarly, it was also predicted that modal Raman gain of HIS-WGs should be higher than expected from the scalar model [49].

Here, we extend the vectorial model to investigate the nonlinear interaction of the two polarizations of a guided mode. The full vectorial model leads to an induced anisotropy on the dynamics of the nonlinear interaction of the two polarizations [50], which we refer to as structurally induced anisotropy, in order to differentiate this anisotropy from others, such as those for which the anisotropy originates from isotropic materials. The origin of the anisotropy is the structure of the waveguide rather than the waveguide material.

The origin of this anisotropy in subwavelength and high index contrast waveguides has also been reported by Daniel and Agrawal [35], who considered nonlinear interactions of the two polarizations in a silicon rectangular nanowire including the effect of free carriers. In their analysis, however, they ignore the coherent coupling of the two polarizations, considering the dynamics of the Stokes parameters only for a specific waveguide and ignore the linear phase.

This anisotropy in turn leads to a new parameter space in which the interaction of the two polarizations shows switching behavior, which is a feature of the vectorial model not accessible through the scalar model with the underlying weak guidance approximation. We also show that the resulting system of nonlinear equations, for the static case, can be solved analytically. Due to the underlying similarity of the nonlinear interaction of the two polarizations and the nonlinear directional coupling of two waveguides, the anisotropy discussed here can be also applied to the case of nonlinear directional coupling, in which the two waveguides have different effective nonlinear coefficients for the propagating modes.

This work develops and expands on results reported in [50, 51], but in addition we derive (in Section 2) the equations that describe the nonlinear interactions of the two polarizations within the framework of the vectorial model, including all relevant nonlinear terms, with explicit integral expressions for all the nonlinear coefficients. In Section 3 we determine properties of the static solutions, classify the steady state solutions, and determine their stability using a Lagrangian formalism. We also discuss a Hamiltonian approach and how the phase space portrait provides a complete picture of the trajectories of the system, including the periodic and solitonic solutions (Section 3.5), and the relevance of the separatrix to the switching solutions. We derive analytical periodic solutions by direct integration of the system of equations in Section 4, and then discuss switching solutions and their properties. We relegate to the Appendix a mathematical analysis of the exact soliton solutions, which are relevant to the switching solutions, with concluding remarks in Section 5.

#165808 - $15.00 USD Received 30 Mar 2012; revised 27 May 2012; accepted 30 May 2012; published 14 Jun 2012

2. Nonlinear differential equations of the model

In the vectorial model the nonlinear pulse propagation of different modes of a waveguide is described by the equations:

$$\begin{aligned}\frac{\partial A_\nu}{\partial z} &+ \sum_{n=1}^{\infty}\frac{i^{n-1}\beta_\nu^{(n)}}{n!}\frac{\partial^n A_\nu}{\partial t^n}\\ &= i\left(\gamma_\nu\left|A_\nu\right|^2+\gamma_{\mu\nu}\left|A_\mu\right|^2\right)A_\nu + i\gamma'_{\mu\nu}A_\mu^2A_\nu^*e^{-2i(\beta_\nu-\beta_\mu)z}+i\gamma_{\mu\nu}^{(1)}A_\mu^*A_\nu^2e^{-i(\beta_\mu-\beta_\nu)z}\\ &\quad +i\gamma_{\mu\nu}^{(2)}A_\mu\left|A_\nu\right|^2e^{i(\beta_\mu-\beta_\nu)z}+i\gamma_{\mu\nu}^{(3)}A_\mu\left|A_\mu\right|^2e^{i(\beta_\mu-\beta_\nu)z} \qquad (2)\end{aligned}$$

where $\mu,\nu=1,2$ with $\mu\neq\nu$, and $A_1(z,t),A_2(z,t)$ are the amplitudes of the two orthogonal polarizations. These equations follow from the analysis in [33], by combining Eqs. (23) and (32) of [33], but without the shock term. The linear birefringence is defined by $\Delta\beta_{\nu\mu}=-\Delta\beta_{\mu\nu}=\beta_\nu-\beta_\mu$ and the γ coefficients are given by

$$\gamma_\nu = \left(\frac{k\varepsilon_0}{4\mu_0}\right)\frac{1}{3N_\nu^2}\int n^2(x,y)n_2(x,y)\left[2\left|\mathbf{e}_\nu\right|^4+\left|\mathbf{e}_\nu^2\right|^2\right]\mathrm{d}A, \qquad (3)$$

$$\gamma_{\mu\nu} = \left(\frac{k\varepsilon_0}{4\mu_0}\right)\frac{2}{3N_\nu N_\mu}\int n^2(x,y)n_2(x,y)\left[\left|\mathbf{e}_\nu\centerdot\mathbf{e}_\mu^*\right|^2+\left|\mathbf{e}_\nu\centerdot\mathbf{e}_\mu\right|^2+\left|\mathbf{e}_\nu\right|^2\left|\mathbf{e}_\mu\right|^2\right]\mathrm{d}A, \qquad (4)$$

$$\gamma'_{\mu\nu} = \left(\frac{k\varepsilon_0}{4\mu_0}\right)\frac{1}{3N_\nu N_\mu}\int n^2(x,y)n_2(x,y)\left[2(\mathbf{e}_\mu\centerdot\mathbf{e}_\nu^*)^2+(\mathbf{e}_\mu)^2(\mathbf{e}_\nu)^2\right]\mathrm{d}A, \qquad (5)$$

$$\gamma_{\mu\nu}^{(1)} = \left(\frac{k\varepsilon_0}{4\mu_0}\right)\frac{1}{3\sqrt{N_\nu^3N_\mu}}\int n^2(x,y)n_2(x,y)\left[2\left|\mathbf{e}_\nu\right|^2(\mathbf{e}_\mu^*\centerdot\mathbf{e}_\nu)+(\mathbf{e}_\nu)^2(\mathbf{e}_\mu^*\centerdot\mathbf{e}_\nu^*)\right]\mathrm{d}A, \qquad (6)$$

$$\gamma_{\mu\nu}^{(2)} = \left(\frac{k\varepsilon_0}{4\mu_0}\right)\frac{2}{3\sqrt{N_\nu^3N_\mu}}\int n^2(x,y)n_2(x,y)\left[2\left|\mathbf{e}_\nu\right|^2(\mathbf{e}_\mu\centerdot\mathbf{e}_\nu^*)+(\mathbf{e}_\nu^*)^2(\mathbf{e}_\mu\centerdot\mathbf{e}_\nu)\right]\mathrm{d}A, \qquad (7)$$

$$\gamma_{\mu\nu}^{(3)} = \left(\frac{k\varepsilon_0}{4\mu_0}\right)\frac{1}{3\sqrt{N_\mu^3N_\nu}}\int n^2(x,y)n_2(x,y)\left[2\left|\mathbf{e}_\mu\right|^2(\mathbf{e}_\mu\centerdot\mathbf{e}_\nu^*)+(\mathbf{e}_\mu)^2(\mathbf{e}_\mu^*\centerdot\mathbf{e}_\nu^*)\right]\mathrm{d}A. \qquad (8)$$

Here we use the notation $(\mathbf{e}_\nu)^2=\mathbf{e}_\nu\centerdot\mathbf{e}_\nu$, $|\mathbf{e}_\nu|^2=\mathbf{e}_\nu\centerdot\mathbf{e}_\nu^*$ and $\left|\mathbf{e}_\nu^2\right|^2=(\mathbf{e}_\nu\centerdot\mathbf{e}_\nu)(\mathbf{e}_\nu^*\centerdot\mathbf{e}_\nu^*)$, together with $\left|\mathbf{e}_\nu\centerdot\mathbf{e}_\mu^*\right|^2=(\mathbf{e}_\nu.\mathbf{e}_\mu^*)(\mathbf{e}_\nu^*\centerdot\mathbf{e}_\mu)$. In these equations $\mathbf{e}_1(x,y),\mathbf{e}_2(x,y)$ are the modal fields of the two orthogonal polarizations, $k=2\pi/\lambda$ is the propagation constant in vacuum, and γ_ν, $\gamma_{\mu\nu}$, $\gamma'_{\mu\nu}$, $\gamma_{\mu\nu}^{(1)}$, $\gamma_{\mu\nu}^{(2)},\gamma_{\mu\nu}^{(3)}$ are the effective nonlinear coefficients representing, respectively, self phase modulation, cross phase modulation, and coherent coupling of the two polarizations, and

$$N_\mu=\frac{1}{2}\left|\int\mathbf{e}_\mu\times\mathbf{h}_\mu^*\centerdot\widehat{\mathbf{z}}\,\mathrm{d}A\right| \qquad (9)$$

is the normalization parameter.

The coupled Eqs. (2) describe the full vectorial nonlinear interaction of the two polarizations. There are two fundamental differences between these equations and the typical scalar coupled Schrödinger equations (see for example Chapter 6 in [32]). Firstly, the additional terms $A_\mu^*A_\nu^2,A_\mu\left|A_\nu\right|^2,A_\mu\left|A_\mu\right|^2$ on the right hand side of Eq. (2) represent interactions between the two polarizations. These do not appear in the scalar model since the effective nonlinear coefficients associated with these terms, $\gamma_{\mu\nu}^{(1)},\gamma_{\mu\nu}^{(2)},\gamma_{\mu\nu}^{(3)}$ as given in Eqs. (6)–(8), contain factors such as $\mathbf{e}_\mu\centerdot\mathbf{e}_\nu$ which are zero in the scalar model, since the modes are assumed to be

#165808 - $15.00 USD Received 30 Mar 2012; revised 27 May 2012; accepted 30 May 2012; published 14 Jun 2012

purely transverse. All possible third power combinations of the two polarization fields, namely $|A_\nu|^2 A_\nu, |A_\mu|^2 A_\nu, A_\mu^2 A_\nu^*, A_\mu^* A_\nu^2, A_\mu |A_\nu|^2$ and $A_\mu |A_\mu|^2$ occur on the right hand side of Eq. (2), due to the z-component of the modal fields. Secondly, in all effective nonlinear coefficients given by Eqs. (3)–(8), the modal fields **e** and **h** have both transverse and longitudinal components, unlike the scalar model in which modal fields have only transverse components. The terms containing nonzero $\mathbf{e}_\mu \cdot \mathbf{e}_\nu$ provide a mechanism for the interaction of the two polarizations since they allow for exchange of power between the two modes through the z-components of their fields. The last term on the right hand side of Eq. (2), for example, indicates a coupling of power into a polarization, even if initially no power is coupled into that polarization.

Although the terms on the right hand side of Eq. (2) that contain $\mathbf{e}_\mu \cdot \mathbf{e}_\nu$ are nonzero, they are generally significantly smaller than the remaining terms and are therefore neglected in the following; further investigation of the effects of these terms, and a discussion of their physical significance, will be presented elsewhere. The focus of this paper is to investigate the effect of the z-components of the fields **e** and **h**, which influence the values of the effective coefficients, and therefore also the nonlinear interactions of the two polarizations. Hence, from Eq. (2), we obtain the equations:

$$\frac{\partial A_\nu}{\partial z} + \sum_{n=1}^{\infty} \frac{i^{n-1}}{n!} \beta_\nu^{(n)} \frac{\partial^n A_\nu}{\partial t^n} = i\left(\gamma_\nu |A_\nu|^2 + \gamma_{\mu\nu} |A_\mu|^2\right) A_\nu + i\gamma'_{\mu\nu} A_\mu^2 A_\nu^* e^{-2i(\beta_\nu - \beta_\mu)z}. \tag{10}$$

These are similar in form to the scalar coupled equations ([32], Section 6.1.2), however, the coefficients $\gamma_\nu, \gamma_{\mu\nu}, \gamma'_{\mu\nu}$, given in Eqs. (3)–(5), now contain z-components of the electric field, through both **e** and **h**. In the framework of the scalar model, the weak guidance approximation assumes that the effective mode areas of the two polarization modes are equal [32], leading to

$$\gamma_1 = \gamma_2 = 3\gamma_c/2 = 3\gamma'_c, \tag{11}$$

where we have denoted $\gamma_c = \gamma_{12} = \gamma_{21}, \gamma'_c = \gamma'_{12} = \gamma'_{21}$. This means that in the scalar model there is an isotropy of the nonlinear interaction of the two polarizations; in order to break this isotropy, one needs to use either anisotropic waveguide materials or twisted fibers, or else couple varying light powers into the two polarizations by using either counter- or co-propagating laser beams. The fact that in the vectorial form Eq. (10) of the coupled equations the γ values include the z-component of the fields, as given by Eqs. (3)–(5), means that Eqs. (11) do not hold in general. As an example, see Fig. 1 in [50] which plots $\gamma_1, \gamma_2, \gamma_c, \gamma'_c$ for a step-index glass-air waveguide with an elliptical cross section; evidently Eqs. (11) are not satisfied. One consequence of the vectorial formulation is, as we show in Section 3.4, the existence of unstable states not present in the scalar formulation.

3. Static equations

We find now all solutions of Eq. (10) for the static case, in which the fields A_1, A_2 are functions of z only. We have therefore the two equations

$$\frac{dA_1}{dz} = i\left(\gamma_1 |A_1|^2 + \gamma_c |A_2|^2\right) A_1 + i\gamma'_c A_2^2 A_1^* e^{-2i\Delta\beta z} \tag{12}$$

$$\frac{dA_2}{dz} = i\left(\gamma_2 |A_2|^2 + \gamma_c |A_1|^2\right) A_2 + i\gamma'_c A_1^2 A_2^* e^{2i\Delta\beta z}, \tag{13}$$

where $\Delta\beta = \beta_1 - \beta_2$. We express the fields A_1, A_2 in polar form according to

$$A_1 = \sqrt{P_1}\, e^{i\phi_1}, \qquad A_2 = \sqrt{P_2}\, e^{i\phi_2}, \tag{14}$$

#165808 - $15.00 USD Received 30 Mar 2012; revised 27 May 2012; accepted 30 May 2012; published 14 Jun 2012

where the powers P_1, P_2 and the phases ϕ_1, ϕ_2 are real functions of z. It is convenient to define the phase difference $\Delta\phi$ and an angle θ according to

$$\Delta\phi = \phi_1 - \phi_2 + z\Delta\beta, \qquad \theta = 2\Delta\phi, \tag{15}$$

then upon substitution into Eqs. (12) and (13) we obtain the four real equations:

$$\frac{dP_1}{dz} = 2\gamma_c' P_1 P_2 \sin\theta \tag{16}$$

$$\frac{dP_2}{dz} = -2\gamma_c' P_1 P_2 \sin\theta \tag{17}$$

$$\frac{d\theta}{dz} = 2\Delta\beta + 2P_1(\gamma_1 - \gamma_c - \gamma_c'\cos\theta) - 2P_2(\gamma_2 - \gamma_c - \gamma_c'\cos\theta) \tag{18}$$

$$\frac{d\phi_1}{dz} = \gamma_1 P_1 + P_2(\gamma_c + \gamma_c'\cos\theta). \tag{19}$$

The last equation decouples from the remaining equations, hence we first solve Eqs. (16)–(18) for P_1, P_2, θ and then determine ϕ_1 by integrating Eq. (19). Equations (16) and (17) show that $P_0 = P_1 + P_2$ is constant in z. We define the dimensionless variables

$$v = \frac{P_1}{P_0} = \frac{P_1}{P_1 + P_2}, \qquad \tau = 2\gamma_c' P_0 z, \tag{20}$$

and the dimensionless parameters

$$a = -\frac{\Delta\beta}{\gamma_c' P_0} - \frac{\gamma_c - \gamma_2}{\gamma_c'}, \qquad b = \frac{\gamma_1 + \gamma_2 - 2\gamma_c}{2\gamma_c'}. \tag{21}$$

In terms of these parameters we obtain the two equations:

$$\dot{v} \equiv \frac{dv}{d\tau} = v(1-v)\sin\theta, \tag{22}$$

$$\dot{\theta} \equiv \frac{d\theta}{d\tau} = -a + 2bv + (1-2v)\cos\theta. \tag{23}$$

Since τ takes only positive values, we may regard τ as a time variable which is limited in value only by the length of the optical fiber and by the value of P_0, and we set the initial values $v_0 = v(0), \theta_0 = \theta(0)$ at time $\tau = 0$, i.e. at one end of the fiber. The general solution depends on the initial values v_0, θ_0 and on only two parameters a, b, even though Eqs. (16)–(19) depend on the five constants $P_0, \gamma_1, \gamma_2, \gamma_c, \gamma_c'$.

At the initial time we have $P_1, P_2 > 0$ and so we always choose v_0 such that $0 < v_0 < 1$. It may be shown from Eqs. (22) and (23) that $0 < v(\tau) < 1$ is then maintained for all $\tau > 0$, i.e. the powers P_1, P_2 remain strictly positive at all later times. The constraint $0 < v_0 < 1$ implies that the initial speed $\dot{\theta}_0$ is restricted, since it follows from Eq. (23) that $|\dot{\theta}| \leqslant |a| + 2|b| + 1$ at all times τ.

3.1. Properties of a, b

Of the two dimensionless parameters a, b, evidently b depends only on the optical fiber parameters, whereas a depends also on the total power P_0, unless $\Delta\beta = 0$. For the scalar model, when Eqs. (11) are satisfied, we have $b = 1$ but generally $b \neq 1$. In this case a set of steady state solutions appears (the states Eq. (24) discussed in Section 3.2 below) which for certain values of a, b are unstable. For fibers with elliptical cross sections we find that $b > 1$ and the unstable

#165808 - $15.00 USD Received 30 Mar 2012; revised 27 May 2012; accepted 30 May 2012; published 14 Jun 2012

steady states exist provided $1 < a < 2b-1$. We have not, however, been able to eliminate the possibility that $b < 1$ for other geometries, and so in the following we also analyze the case $b < 1$. The parameter a can be positive or negative depending on the sign of $\Delta\beta$ and on the value P_0; when Eqs. (11) are satisfied we have $a = -3\Delta\beta/(P_0\gamma_1)+1$ and hence a can take large positive or negative values for small P_0.

As an example, we have evaluated b using the definitions Eqs. (3)–(5) for step-index, air-clad glass waveguides with elliptical cross sections where the major/minor axes are denoted x,y. The host glass is taken to be chalcogenide with linear and nonlinear refractive indices of $n = 2.8$ and $n_2 = 1.1\times10^{-17}\text{m}^2/\text{W}$ at $\lambda = 1.55\mu\text{m}$ (as in [52]). Figure 1(i) shows a contour plot of $\log_{10} b$ as a function of x,y. We see, as expected, that b approaches 1 as the waveguide dimensions x,y increase towards the operating wavelength. For small core waveguides, however, we find $b > 1$ with values as large as $b \approx 200$. The parameter a, on the other hand, depends on both the structure and the total input power P_0. For low input powers, specifically for $P_0\gamma_c' \ll |\Delta\beta|$, a can take large negative values (for $\Delta\beta > 0$) or positive values (for $\Delta\beta < 0$) as shown in Fig. 1(ii). For large values of P_0, however, a approaches the constant $C = (\gamma_2-\gamma_c)/\gamma_c'$, whose contours for elliptical core waveguides are shown in Fig. 1(iii); most such waveguides have positive C values ranging up to 400, but some, those in the region on the left side of the white curve in Fig. 1(iii), have negative or small values of C. The contour plot for $\Delta\beta$ in Fig. 1(iv) shows that $\Delta\beta$ takes a wide range of positive and negative values as x,y vary.

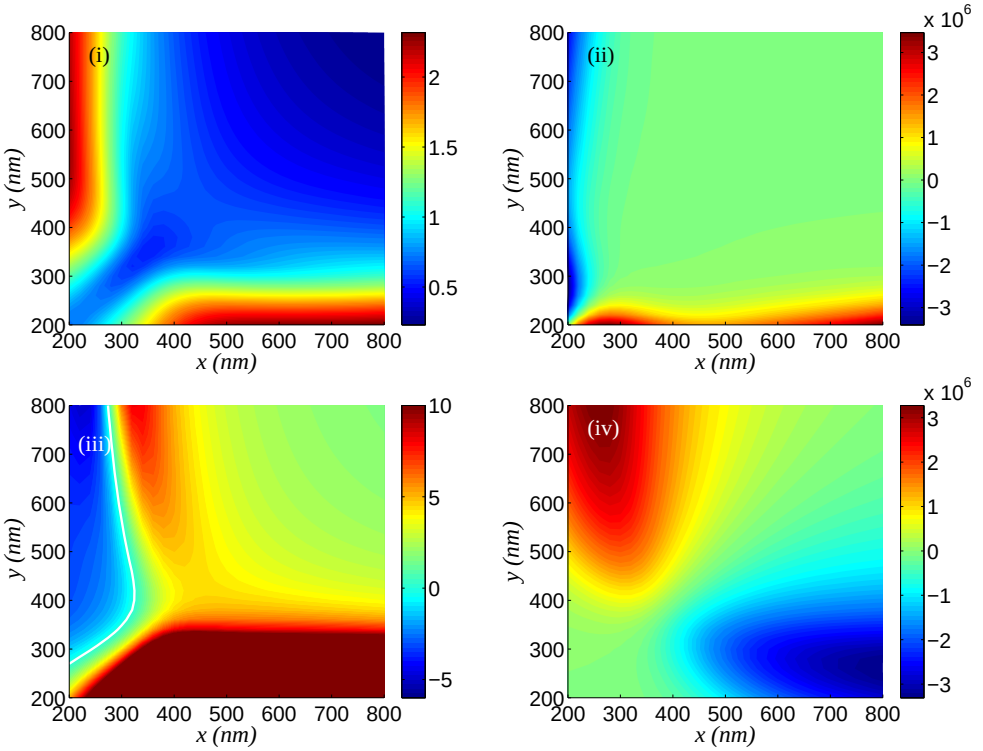

Fig. 1. Contour plots as functions of the elliptical waveguide dimensions x,y of (i) $\log_{10} b$; (ii) a as defined in Eq. (21) for $P_0 = 1\text{W}$; (iii) $C = (\gamma_2-\gamma_c)/\gamma_c'$ where $C < 0$ to the left of the white line; (iv) the birefringence $\Delta\beta$.

#165808 - $15.00 USD Received 30 Mar 2012; revised 27 May 2012; accepted 30 May 2012; published 14 Jun 2012

3.2. Steady state solutions

There are four classes of steady state solutions of Eqs. (22) and (23), each of which exist only for values of a, b within certain limits, as follows:

$$\cos\theta = 1, \quad v = \frac{a-1}{2(b-1)} \tag{24}$$

provided $b \neq 1$ and $0 < \frac{a-1}{2(b-1)} < 1$;

$$\cos\theta = -1, \quad v = \frac{a+1}{2(b+1)} \tag{25}$$

provided $b \neq -1$ and $0 < \frac{a+1}{2(b+1)} < 1$;

$$\cos\theta = a, \quad v = 0 \tag{26}$$

provided $|a| \leqslant 1$; and

$$\cos\theta = -a + 2b, \quad v = 1 \tag{27}$$

provided $|a - 2b| \leqslant 1$.

Of these four classes, the values Eqs. (26) and (27) lie on the boundary of the physical region $0 < v < 1$, but nevertheless influence properties of nearby nontrivial trajectories, and also play a role in soliton solutions. The states Eq. (24) lie within the physical region only if the parameters (a, b) belong to either the red or green region of the a, b plane shown in Fig. 2(i). Similarly the solutions Eq. (25) satisfy $0 < v < 1$ only in the disjoint regions of the a, b plane defined by either $2b + 1 < a < -1$ or $-1 < a < 2b + 1$. If a, b lie outside these regions, and also outside the strips given by $|a| \leqslant 1$ and $|a - 2b| \leqslant 1$, there are no steady state solutions.

For special values of a, b these steady states can coincide, for example if $a = 1$ the solution Eq. (26) coincides with the boundary value of Eq. (24). Steady states for values of a, b on the boundary of the regions shown in Fig. 2 may need to be considered separately; for example if $a = b = 1$ then all steady states are given either by Eq. (25), or else by $\cos\theta = 1$ and any constant v.

In practice, the values of a, b are determined by the waveguide structure, the propagating mode and, in the case of a, the input power P_0, and hence only restricted regions of the a, b plane are generally accessible. For example, Fig. 1(i) shows that for the fundamental mode of elliptical core fibers we have $\log_{10} b \geqslant 0$, and so the attainable values of b are limited to $b \geqslant 1$. We nevertheless include the case $b < 1$ in our analysis, since this possibility cannot be excluded for other fiber geometries. We discuss the accessible regions for the case of unstable steady states in Section 3.4.

3.3. Lagrangian formulation

We wish to determine the stability properties of each of the four classes of steady state solutions, in particular we look for unstable steady states. These are of interest because polarization states which lie close to these unstable states are very sensitive to small changes in parameters such as the total power P_0, and so can flip abruptly as a function of the optical fiber length z. Although we may determine stability properties by investigating perturbations about the constant solutions, we find it convenient to reformulate the defining Eqs. (22) and (23) as the Euler-Lagrange equations of a Lagrangian L which is a function of $\theta, \dot{\theta}$, and depends otherwise only on the parameters a, b. This also provides insight into the properties and solutions of these equations,

#165808 - $15.00 USD Received 30 Mar 2012; revised 27 May 2012; accepted 30 May 2012; published 14 Jun 2012

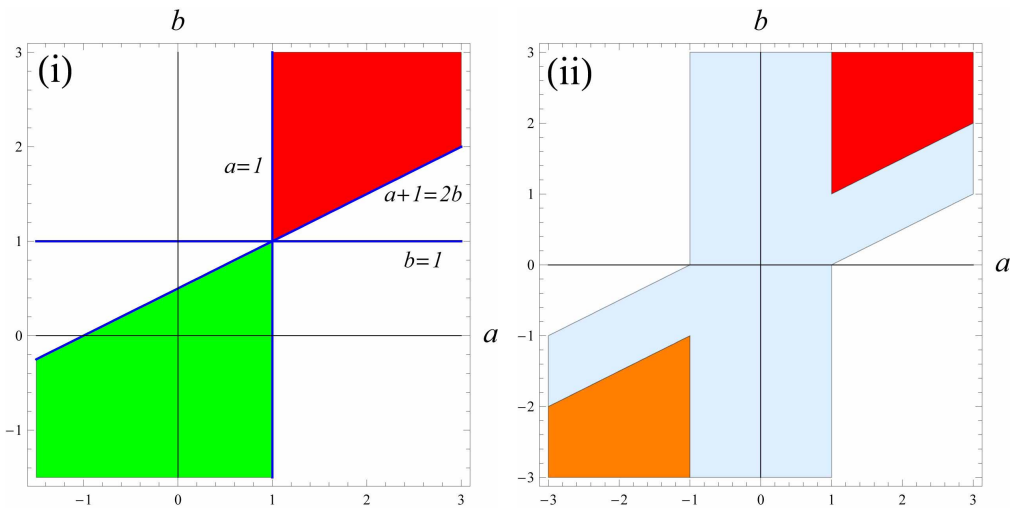

Fig. 2. The a,b plane showing: (i) the regions of existence for the solutions Eq. (24), either $1<a<2b-1$ (red), or $2b-1<a<1$ (green); (ii) the regions of existence for the *unstable* solutions consisting of Eq. (24) (red), and Eq. (25) for which $2b+1<a<-1$ (orange), together with Eqs. (26) and (27) for which $|a|<1$ or $|a-2b|<1$ (light blue).

and we may then investigate stability by examining the corresponding potential function. From Eq. (23) we have

$$v=\frac{\dot\theta+a-\cos\theta}{2(b-\cos\theta)}, \tag{28}$$

and by substitution into Eq. (22) we obtain

$$2(b-\cos\theta)\,\ddot\theta-\sin\theta\,\dot\theta^2+\sin\theta(a-\cos\theta)(a-2b+\cos\theta)=0. \tag{29}$$

We consider Lagrangians L of the form

$$L=T-V=\frac{1}{2}M(\theta)\,\dot\theta^2-V(\theta) \tag{30}$$

where T is the (positive) kinetic energy, V is the potential energy, and the "mass" M is a positive function of θ. The equation of motion is

$$M(\theta)\,\ddot\theta+\frac{1}{2}M'(\theta)\dot\theta^2+V'(\theta)=0, \tag{31}$$

and is identical to Eq. (29) provided

$$M(\theta)=\frac{2}{|b-\cos\theta|},\qquad V(\theta)=-|b-\cos\theta|-\frac{(a-b)^2}{|b-\cos\theta|}. \tag{32}$$

We may therefore investigate all possible solutions $\theta(\tau)$ by analyzing properties of the periodic potential $V(\theta)$; every solution of the system of Eqs. (22) and (23) corresponds to the trajectory $\theta(\tau)$ of a particle of variable mass M in the potential V. Steady state solutions are zeroes of $V'(\theta)$, and stability is determined by whether these zeroes are local maxima or minima of V, subject to the constraint that the associated function v should always satisfy $0<v<1$. Trajectories which begin near a local minimum, with a small initial speed $\dot\theta(0)$, oscillate periodically with a small amplitude. On the other hand, trajectories which begin near an unstable

#165808 - $15.00 USD Received 30 Mar 2012; revised 27 May 2012; accepted 30 May 2012; published 14 Jun 2012

point, i.e. near a local maximum of V, can display periodic oscillations of large amplitude with abrupt transitions between adjacent local maxima; we refer to these as switching solutions (previously bistable solutions [50]) since $\cos\Delta\phi = \cos(\theta/2)$ switches periodically between two distinct values. Soliton trajectories also occur in which the particle moves between adjacent local maxima of V, see for example the discussion in [53], Section 2 and [54] for properties of solitons in optical fibers. As mentioned in Section 3.5, soliton trajectories also appear as the separatrix in phase plane plots.

We plot V as a function of θ and either a or b in Fig. 3, showing that V defines a complex surface with valleys and peaks which change suddenly as a or b are varied. Periodic solutions occur for trajectories restricted to a local valley, but there are also unbounded trajectories, in which θ increases or decreases indefinitely, depending on a, b and on whether $\dot\theta(0)$ is sufficiently large. The potential, as a function of θ and a, has saddle points which indicate that a stable solution can become unstable as a is varied; according to the definition Eq. (21) we may vary a within certain limits by varying the total power P_0.

For $a = b$ the potential is essentially that of the nonlinear pendulum under the influence of gravity, namely a simple cosine potential, but with a mass that depends on θ. Provided $b > 1$ this mass varies between two positive, finite limits. The unstable steady states correspond to a pendulum balanced upright, while the switching states (discussed in Section 4) correspond to trajectories which begin with the pendulum positioned near the top, possibly with a small initial speed, then swinging rapidly through $\theta = 2\pi$ to reach the adjacent unstable steady state. During this motion $\cos\Delta\phi = \cos\frac{\theta}{2}$ flips rapidly between the values ± 1. The soliton discussed in the Appendix is the trajectory in which the pendulum begins at the unstable upright position and, over an infinite time, moves through the stable minimum to the adjoining unstable steady state.

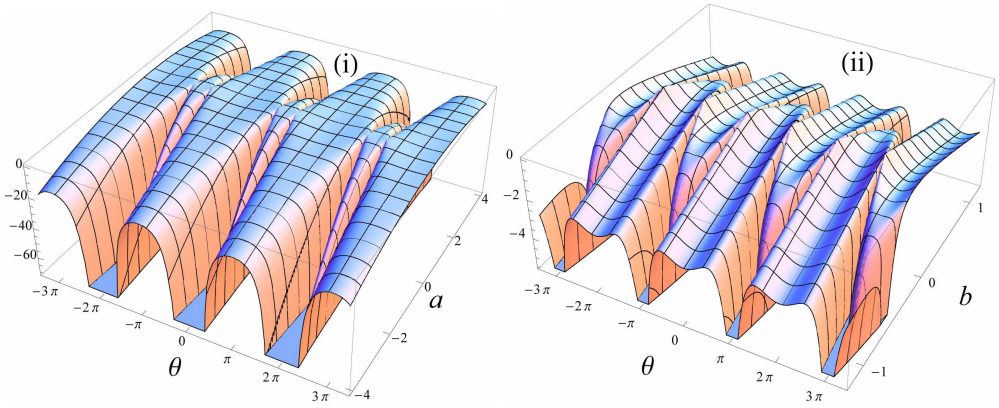

Fig. 3. The potential V plotted as a function of (i) θ, a for $b = 0.8$; (ii) θ, b for $a = 0$.

Although both M and V are singular when $\cos\theta = b$, which occurs only if $|b| \leqslant 1$, this singularity is an artifact of the Lagrangian formulation, as is evident from Eqs. (22) and (23), which have smooth bounded right hand sides for any b. In particular v, which is obtained from Eq. (28) given θ, is a smooth function of τ even if $\cos\theta = b$ for some τ.

The energy $T + V = \frac{1}{2}M(\theta)\,\dot\theta^2 + V(\theta)$ is a constant of the motion. Hence we may integrate Eq. (29) to obtain

$$\dot\theta^2 = (b - \cos\theta)^2 + (a - b)^2 + c\,(b - \cos\theta), \tag{33}$$

where c is the constant of integration. This constant is determined by first choosing initial values v_0, θ_0, where $0 < v_0 < 1$, and then finding $\dot\theta(0)$ from Eq. (23) which, from Eq. (33) evaluated at

#165808 - $15.00 USD Received 30 Mar 2012; revised 27 May 2012; accepted 30 May 2012; published 14 Jun 2012

$\tau = 0$, fixes c. We may integrate Eq. (33) to determine θ as an explicit function of τ, expressible in terms of elliptic functions, as discussed further in Section 3.5.

A limitation of the Lagrangian formulation is that the constraint $0 < v < 1$ is not easily implemented. Whereas every solution of the system Eqs. (22) and (23) defines a trajectory $\theta(\tau)$ in the Lagrangian system Eq. (29), the converse is not true, i.e not all trajectories in this system satisfy $0 < v < 1$. The initial speed $\dot{\theta}(0)$ must be restricted to only those values allowed by Eq. (23), in which $0 < v(0) < 1$, and similarly the constant solutions of Eq. (29) are valid steady states for the original Eqs. (22) and (23) only in certain regions of the a, b plane. Trajectories which violate $0 < v < 1$, while not physical in the context of optical fiber configurations, can nevertheless be viewed as acceptable motions of the mechanical system defined by the Lagrangian Eq. (30). We investigate an alternative Hamiltonian formulation in terms of v in Section 3.5.

3.4. Stability of steady state solutions

The stability of each of the four classes of steady state solutions in Section 3.2 is determined by the sign of V'' for that solution; a positive sign implies that the solution lies at a local minimum of V and is therefore stable, whereas a negative sign implies that the solution is unstable.

For the steady states Eq. (24) we have $V'' = (a-1)(a-2b+1)(b-1)/|b-1|^3$ and so these states are stable for points a, b such that $(a-1)(a-2b+1)(b-1 > 0$, shown as the green region in the a, b plane in Fig. 2(i), and are unstable in the red region, where $1 < a < 2b-1$. For the steady states Eq. (25) we have $V'' = (a+1)(-a+2b+1)(b+1)/|b+1|^3$ and so these solutions are stable for $-1 < a < 2b+1$ and are unstable in in the orange region $2b+1 < a < -1$ shown in Fig. 2(ii).

For the remaining steady states Eqs. (26) and (27), for which $v = 0$ or $v = 1$, we have $V'' = -2\sin^2\theta/|a-b|$ which in all cases is negative, and so these states are unstable whenever they exist. This is consistent with the observation that $v(\tau)$ cannot attain the values $0, 1$ at any time τ, provided $0 < v_0 < 1$. The regions in the a, b plane where the unstable states exist are shown in Fig. 2(ii).

Next, we determine conditions under which the unstable steady state solutions Eq. (24) are accessible. For elliptical core step index fibers, for which $b > 1$ as shown in Fig. 1(i), the region of instability is indeed accessible and leads to properties such as nonlinear self-polarization flipping, discussed in Section 4. The region of unstable solutions is given by $1 < a < 2b-1$, equivalently

$$\gamma_c + \gamma_c' - \gamma_1 < \frac{\Delta\beta}{P_0} < \gamma_2 - \gamma_c - \gamma_c'. \tag{34}$$

These inequalities specify the possible values, if any, of P_0 for which the unstable solutions exist for a fixed fiber. In order to visualize this region we plot a as a function of P_0 in Fig. 4(i), where a is given by Eq. (21). The boundaries of the unstable region at $a = 1, a = 2b-1$ are shown by the green solid lines.

First we consider fibers for which $1 < C < 2b-1$, where $C = (\gamma_2 - \gamma_c)/\gamma_c'$ takes the value shown by the dashed line in Fig. 4(i). Then a has two branches associated with either $\Delta\beta < 0$ or $\Delta\beta > 0$; for the branch corresponding to $\Delta\beta < 0$ (the solid blue line), a is large and positive for small P_0 and asymptotically approaches C for large P_0. The intersection of this branch with the boundary $a = 2b-1$ determines the minimum power $P_{\min_1}$ required in order to access the unstable region. In this case, only part of the unstable region corresponding to $C < a < 2b-1$ is accessible, as shown by the blue region. For the $\Delta\beta > 0$ branch (red solid curve) a is large and negative for small P_0 and asymptotically approaches C for large P_0. For this branch, P_0 needs to be larger than a value $P_{\min_2}$. The unstable region is accessible provided $1 < a < C$ and is a subset (red shaded) of the whole unstable solution region. Figure 4(i) allows one to determine

#165808 - $15.00 USD Received 30 Mar 2012; revised 27 May 2012; accepted 30 May 2012; published 14 Jun 2012

the minimum and maximum values of a and the minimum power to access the unstable solution region, once $\Delta\beta$ and C are known. For elliptical core fibers these two values are completely determined by the dimensions x, y, see Fig. 1(iii,iv) for plots of C and $\Delta\beta$.

Besides fibers for which $1 < C < 2b-1$, there are the possibilities $C > 2b-1$ or $C < 1$. From Fig. 1(iii,iv) one can show that these combinations (with $\Delta\beta$ positive or negative) either do not exist, or do not lead to unstable solutions, since the possible values of a do not lie in the unstable region $1 < a < 2b-1$. In summary, the only elliptical core fibers that allow unstable solutions are those with $1 < C < 2b-1$ with either positive or negative $\Delta\beta$. The case in which $\Delta\beta = 0$ is discussed separately in [55, 56].

Based on the above discussion, one can find the minimum power $P_0^{\min}$ required to generate unstable solutions for elliptical core fibers. Figure 4(ii) plots $\log_{10}(P_0^{\min})$ (where $P_0^{\min}$ is measured in watts) as a function of x, y, where the white region corresponds to fibers for which there are no unstable solutions, and the regions below and above the diagonal line correspond to $P_{\min_1}$ and $P_{\min_2}$, respectively, which have been obtained for the two branches of the function $a(P_0)$ shown in Fig. 4(i). In these examples of elliptical fibers very high powers, in the range $1-10$kW, are required in order to observe switching solutions, as we discuss further in our concluding remarks in Section 5. The underlying theory shows, however, that this behavior can occur at much lower powers for waveguides with small birefringence $\Delta\beta$; specifically, it is necessary only that the inequalities Eq. (34) be satisfied, and so the total power P_0 required is small provided that $\Delta\beta$ is sufficiently small [55].

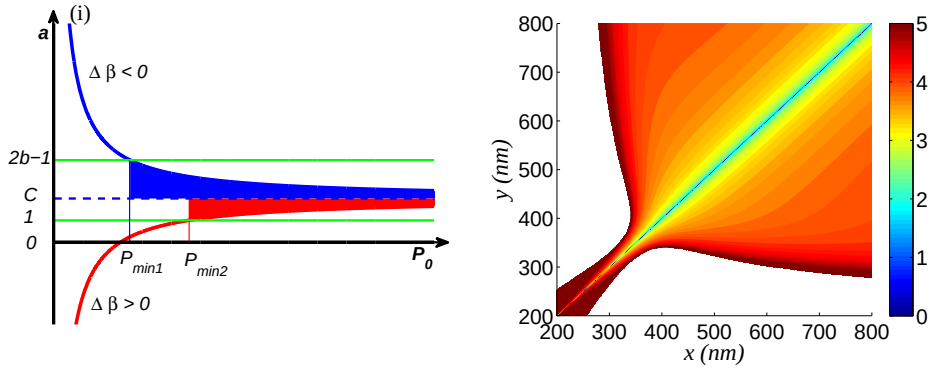

Fig. 4. (i) a as a function of P_0 for $\Delta\beta < 0$ (blue solid line) and $\Delta\beta > 0$ (red solid line). The green lines mark the boundaries of the (red) region of instability in the a, b plane shown in Fig. 2(i); (ii) contour plot of $\log_{10}(P_0^{\min})$ as a function of x, y, showing the minimum total power $P_0^{\min}$ (in units W) required to access unstable steady states, where they exist.

3.5. Hamiltonian function

Although the Lagrangian formulation in terms of θ is convenient for an analysis of the steady states and their stability, and also for a qualitative understanding of all solutions including solitons, the constraint $0 < v < 1$ is more easily implemented by means of a direct formulation in terms of v. This automatically eliminates unphysical trajectories for which one of the input powers P_1, P_2 is negative. Such a formulation follows by construction of a Hamiltonian function which, being conserved, allows us to firstly integrate the nonlinear equations and obtain analytical solutions and, secondly, to interpret physically the possible states of polarizations within an optical waveguide from the phase plane contours. Corresponding to the conserved energy

#165808 - $15.00 USD Received 30 Mar 2012; revised 27 May 2012; accepted 30 May 2012; published 14 Jun 2012

$T+V$ which follows from Eq. (30) there is a Hamiltonian function H defined by

$$H(v,\theta) = -av + bv^2 + v(1-v)\cos\theta \tag{35}$$

which satisfies

$$\dot{v} = -\frac{\partial H}{\partial \theta}, \qquad \dot{\theta} = -\frac{\partial H}{\partial v}.$$

Hence as a function of τ, H is conserved and takes the constant value $H_0 = H(v_0,\theta_0)$ on any trajectory. We may investigate all possible solutions, therefore, by analyzing the curves of constant H_0 in the v,θ plane. We have

$$\cos\theta = \frac{H_0 + av - bv^2}{v(1-v)}, \tag{36}$$

and from Eq. (22) we obtain

$$\dot{v}^2 = Q(v), \tag{37}$$

where Q is the polynomial of 4th degree (provided $b^2 \neq 1$) given by

$$Q(v) = v^2(1-v)^2 - (H_0 + av - bv^2)^2. \tag{38}$$

Since the left hand side of Eq. (37) is positive, solutions exist only if $Q(v) \geqslant 0$ for v in the interval $0 < v < 1$. Generally $Q(0), Q(1) < 0$ but since $Q(v_0) = v_0^2(1-v_0)^2\sin^2\theta_0 \geqslant 0$ (as follows from Eq. (22)) Q has at least two real zeroes, possibly repeated, and so there is an interval within $0 < v < 1$ in which $Q(v) > 0$, and so solutions always exist. If the initial values v_0, θ_0 are such that the trajectory begins in a stable steady state, v remains constant for all $\tau > 0$, otherwise the trajectory is nontrivial. There are two types of nontrivial solutions, periodic and soliton solutions.

We can gain insight into possible solutions by plotting contours of constant $H(v,\theta)$ in the v,θ plane, which supplies essentially a phase portrait of the system. Solutions for which both v,θ are periodic in τ form closed loops, and lie close to a stable steady state, whereas nonperiodic trajectories lie outside the separatrix which defines soliton solutions, as we discuss in the Appendix. Figure 5 shows two examples in which stable steady states are marked in green, and unstable steady states are shown in red or orange. Periodic solutions are evident as closed loops surrounding stable steady states, whereas the separatrix marks soliton trajectories which connect unstable steady states. Apart from these solitons, all other solutions $v, \cos\theta$ (but not necessarily θ) are periodic in τ. The switching solutions of particular interest, in which the state of polarization inside the waveguide flips between two well-defined states, are those close to the separatrix.

4. Periodic solutions

Periodic solutions v of Eq. (37) attain both minimum and maximum values, denoted $v_{\min}, v_{\max}$ respectively, with $0 < v_{\min} \leqslant v_{\max} < 1$. Since $\dot{v} = 0$ at a maximum or minimum of v, both $v_{\min}, v_{\max}$ are roots of Q. We can factorize Q as a product of quadratic polynomials,

$$Q(v) = -\left[(b+1)v^2 - (a+1)v - H_0\right]\left[(b-1)v^2 - (a-1)v - H_0\right], \tag{39}$$

and hence explicitly find all roots, and so identify $v_{\max}$ and $v_{\min}$. We integrate $\dot{v} = \sqrt{Q(v)}$ over the half-period in which v increases, in order to find τ as a function of v, and also the period T:

$$\int_{v_{\min}}^{v} \frac{du}{\sqrt{Q(u)}} = \tau - \tau_0, \quad T = 2\int_{v_{\min}}^{v_{\max}} \frac{du}{\sqrt{Q(u)}}, \tag{40}$$

#165808 - $15.00 USD Received 30 Mar 2012; revised 27 May 2012; accepted 30 May 2012; published 14 Jun 2012

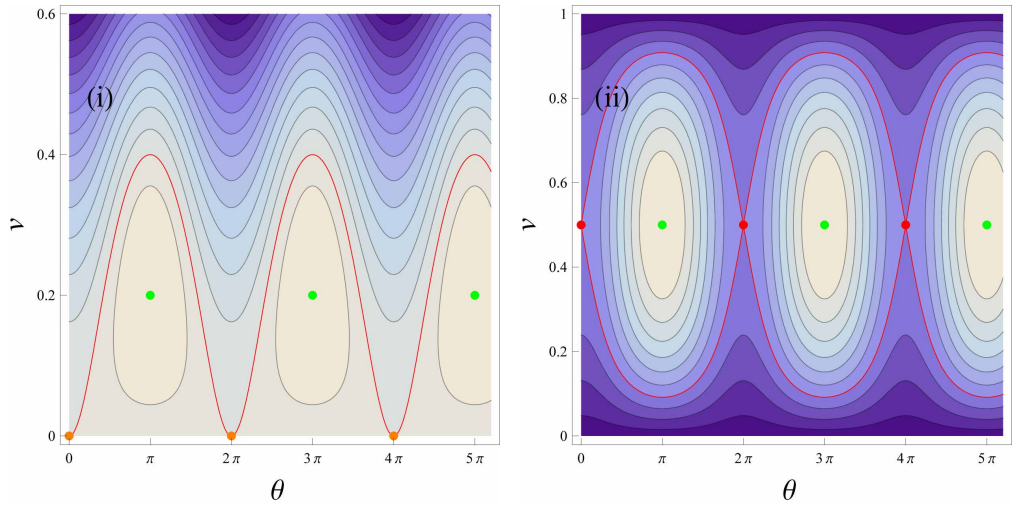

Fig. 5. Contours in the θ, v plane of constant H for (i) $a = 1, b = 4$; (ii) $a = b = 2$, with steady states marked by green dots (stable) and red or orange dots (unstable). The separatrix, which identifies the soliton trajectories, is shown in red.

where τ_0 is the time at which v achieves its minimum, i.e. $v_{\min} = v(\tau_0)$. These integrals may be evaluated in terms of elliptic integrals of the first kind, see for example the explicit formulas in [57] (Sections 3.145, 3.147). In particular, T is expressible in terms of the complete elliptic integral K, and so can be written as an explicit function of a, b, v_0, θ_0, i.e. as a function of the waveguide parameters and the initial power and phase of the input fields. The precise formulas depend on the relative location of the roots of Q.

Having found v, $\cos\theta$ is obtained from Eq. (36) and is also periodic in τ, as is $\dot{\theta}$ which is obtained from Eq. (23), however θ itself need not be periodic. Although it is straightforward to find v, θ numerically as functions of τ, for specified numerical values of a, b and initial values v_0, θ_0, the exact solutions are useful because they display the exact dependence of the solution on all parameters, such as the total power P_0; it is not necessary therefore to solve the equations numerically for every choice of P_0, rather the exact solution gives the explicit periodic solution and the period as known functions of P_0.

For switching solutions, the phase difference between the two polarization vectors experiences abrupt phase shifts through π as the light propagates within the waveguide. As a result, the state of polarization flips between two well-defined polarization states, where the flipping angle depends on a, b and on θ_0, v_0. The following are two examples of switching solutions.

As the first example we choose $a = 1, b = 4$ with the initial values $v_0 = \varepsilon, \theta_0 = 0$, where $\varepsilon = 10^{-4}$, in which case the input laser beam is linearly polarized and the polarization state is close to one of the principle axes of the waveguide. Hence, the trajectory starts near the unstable steady states Eq. (24) or Eq. (26), which lie on the boundary of the red region shown in Fig. 2(i). We plot v and $\cos\frac{\theta}{2} = \cos\Delta\phi$ as a function of τ in Fig. 6(i), showing switching behavior for $\cos\frac{\theta}{2}$, which is periodic and flips abruptly between the values ± 1; θ, however, is an increasing function of τ, with jumps through 2π at periodic intervals. The polarization vector experiences an angular flipping associated with the abrupt flipping of $\cos\Delta\phi$, however, since $v_0 = \varepsilon$ and $\theta_0 = 0$, the flipping angle is very small, as depicted in the inset of Fig. 6(i). Regarded as the trajectory of a particle of mass M in the potential V in Eq. (32) this motion corresponds to a particle moving slowly over the peaks of the potential, which are the unstable steady states, then sliding quickly down the valleys through the minimum values of V and back to the peaks.

#165808 - $15.00 USD Received 30 Mar 2012; revised 27 May 2012; accepted 30 May 2012; published 14 Jun 2012

For $a = 1$ the potential is flat at its maximum values, since in this case $V' = 0 = V'' = V'''$, hence $v, \dot{\theta}$ are each close to zero except when θ moves to an adjoining maximum of V. In terms of the contour plots shown in Fig. 5(i) this trajectory corresponds to the contour which begins just above the unstable steady state (orange dot) and closely follows the separatrix shown in red (which is the soliton solution discussed in the Appendix) with a maximum value ~ 0.4 for v.

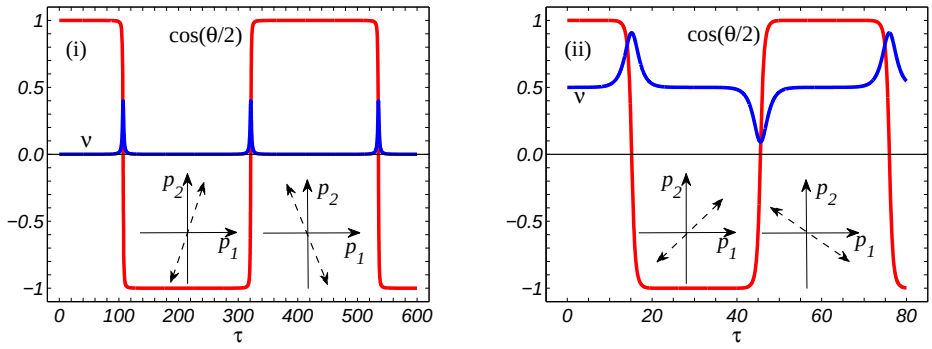

Fig. 6. Switching solutions v and $\cos\frac{\theta}{2} = \cos\Delta\phi$ as functions of τ for: (i) $a = 1, b = 4$ and $v_0 = \varepsilon, \theta_0 = 0$; (ii) $a = b = 2$ and $v_0 = \frac{1}{2}, \theta_0 = \varepsilon$ where $\varepsilon = 10^{-4}$. The insets show the polarization vectors associated with the values $\cos\Delta\phi = \pm 1$.

As a second example of switching behavior we choose $a = b = 2$ with $v_0 = 1/2, \theta_0 = \varepsilon$, where $\varepsilon = 10^{-4}$, which corresponds to a linearly polarized input laser beam in which the polarization vector makes an angle of 45° to either of the principle axes of the waveguide. Again, the initial value lies close to an unstable steady state Eq. (24) and a, b lie within the red region of instability in Fig. 2. We plot v and $\cos(\theta/2)$ as functions of τ in Fig. 6(ii), showing the periodicity of these functions and the switching behavior of $\cos(\theta/2)$. Since $v_0 = 1/2$, the angular flipping of the polarization vector is $\pi/2$, because $\cos(\theta/2)$ flips between values ± 1, as shown in the inset of Fig. 6(ii). Unlike the previous example, θ is also periodic in τ with a trajectory that corresponds to the motion of a particle in the potential V, starting slowly near the unstable steady state Eq. (24) but sliding rapidly through the potential minimum to approach an adjoining unstable steady state. This motion is similar to the periodic oscillations of a nonlinear pendulum (since $a = b$, see the definition of V in Eq. (32)) with a large amplitude of almost 2π, and v attains nearly all values between $0, 1$. In terms of the phase space contours shown in Fig. 5(ii), the motion corresponds to a periodic trajectory which begins near the red dot (unstable steady state) and again closely follows the separatrix which marks the soliton trajectory.

5. Discussion and conclusion

Switching states, as defined and demonstrated here through simulation by means of a full vectorial model, are attractive for practical applications, since they allow nonlinear self-flipping of the polarization states of light propagating in an optical waveguide. This flipping is due to the nonlinear interactions of the two polarizations, and has properties that depend on the total optical power and on the specific fiber parameters. These properties can in principle be employed to construct devices such as optical logic gates [58], fast optical switches and optical limiters [55, 56], in which small controlled changes in the input parameters lead to sudden changes in the polarization states.

The minimum power necessary to generate such switching states is determined for any waveguide by the inequalities Eq. (34) and, for chalcogenide optical nanowires with ellipti-

#165808 - $15.00 USD Received 30 Mar 2012; revised 27 May 2012; accepted 30 May 2012; published 14 Jun 2012

cal core cross sections, is summarized in Fig. 4(ii). The minimum power required in such nanowires is in the range $1-10$kW which, although not practicable for CW lasers, can be achieved in pulsed lasers. Although we have limited our analysis to the static case, ignoring the temporal variation of laser light, it is still applicable to slow pulses with pulse widths in the order of nanoseconds depending on the dispersion of the waveguide. A more practical minimum power requirement that achieves switching behavior is by means of asymmetric waveguides, such as rib waveguides, for which $\Delta\beta$ can be reduced to very small values while still having different field distributions for the two polarizations, as discussed in [55, 56].

The nonlinear interactions of the two polarizations can be impacted by two factors that have not yet been investigated: (1) interactions with higher order modes in few-mode waveguides and, (2) contributions from nonlinear terms containing different forms of $\mathbf{e}_1 \cdot \mathbf{e}_2$, i.e., nonzero values for the coefficients $\gamma_{\mu\nu}^{(1)}, \gamma_{\mu\nu}^{(2)}, \gamma_{\nu}^{(3)}$ in Eqs. (6)–(8). (This applies only when $\mathbf{e}_1 \cdot \mathbf{e}_2$ is no longer very small, as assumed in this paper). In few-mode waveguides, higher order modes contribute to the nonlinear phase of each polarization of the fundamental mode through cross phase and coherent mixing terms. Inspection of Eq. (2) reveals that nonzero $\gamma_{\mu\nu}^{(1)}, \gamma_{\mu\nu}^{(2)}, \gamma_{\mu\nu}^{(3)}$ coefficients significantly change the dynamics of nonlinear interactions of the two polarizations and most likely lead to different parameter regimes for the existence of periodic and solitonic solutions. These factors will be the subject of further studies.

In summary, we have developed the theory of nonlinear interactions of the two polarizations using a full vectorial model of pulse propagation in high index subwavelength waveguides. This theory indicates that there is an anisotropy in the nonlinear interactions of the two polarizations that originates solely from the waveguide structure. We have found all static solutions of the nonlinear system of equations by finding exact constants of integration, which leads to expressions for the general solution in terms of elliptic functions. We have analyzed the stability of the steady state solutions by means of a Lagrangian formalism, and have shown that there exist periodic switching solutions, related to a class of unstable steady states, for which there is an abrupt flipping of the polarization states through an angle determined by the structural parameters of the waveguide and the parameters of the input laser. By means of a Hamiltonian formalism we have analyzed all solutions, including solitons which we have shown are close to the switching solutions of interest.

Appendix

We include here a discussion of the topological solitons which appear as solutions of Eq. (29), as configurations $\theta(\tau)$ which interpolate between the adjacent maxima of the periodic potential V defined in Eq. (32). They define trajectories which move between adjacent unstable steady states with abrupt transitions, to form "kinks" which are stable against time-dependent perturbations. Such trajectories are visible in Fig. 5(i), 5(ii) (the contours marked in red) as they form the separatrix between periodic solutions v, θ and nonperiodic solutions. The fact that solitons can occur in this way has been previously noted, see for example Chapter 9 in [54]. In Fig. 5(i) the soliton is the trajectory which connects the adjacent unstable steady states (orange) at $v = 0$ and $\theta = 0, 2\pi, 4\pi \ldots$ and similarly in Fig. 5(ii) the solitons connect the (red) unstable steady states. Such solutions exist on the full real line $-\infty < \tau < \infty$, with appropriate boundary conditions, but are also solutions on any finite subset of the real line, corresponding to an optical fiber of finite length, with boundary values obtained from the exact solution.

Solitons are significant in the context of switching solutions since switching behavior occurs precisely when solutions lie near soliton trajectories; the switching solutions shown in Fig. 6(i), 6(ii), for example, correspond to contours in Fig. 5(i), 5(ii) which lie very close to the separatrix. The soliton itself is not periodic but nearby trajectories are periodic for both v and $\cos\theta$ as functions of τ. The abrupt transitions which characterize switching, as shown for example in

#165808 - $15.00 USD Received 30 Mar 2012; revised 27 May 2012; accepted 30 May 2012; published 14 Jun 2012

Fig. 6, can equally be viewed as the "kinks" of a soliton, in which $\cos(\theta/2)$ changes between two distinct values over a very short τ-interval, and in doing so interpolates between unstable steady states. We are interested here mainly in transitions between the unstable steady states Eq. (24), since these correspond to polarization flipping, i.e. $\cos\Delta\phi = \cos(\theta/2)$ flips between values ± 1. There exist, however, solitons corresponding to the other unstable steady states such as Eqs. (26) and (27), which we also discuss briefly.

In order to find explicit solutions, we define a potential U according to $U(\theta) = V_0 - V(\theta)$, where the shift V_0 is selected such that the minimum value of U is zero. If $1 < a < 2b-1$, for example, in which case the unstable steady states Eq. (24) exist, we have

$$V_0 = 1 - b - \frac{(a-b)^2}{b-1}. \tag{41}$$

We also define the positive "action" functional S by

$$S(\theta, \dot{\theta}) = \int_{-\infty}^{\infty} \left[\frac{1}{2} M(\theta)\, \dot{\theta}^2 + U(\theta) \right] d\tau. \tag{42}$$

Equations (29) and (31) follow by using Hamilton's principle of least action applied to S. We can write

$$S = \int_{-\infty}^{\infty} \frac{1}{2} M \left[\dot{\theta} \mp \sqrt{\frac{2U}{M}} \right]^2 d\tau \pm \int_{-\infty}^{\infty} M \sqrt{\frac{2U}{M}}\, \dot{\theta}\, d\tau. \tag{43}$$

The last term takes values only on the boundary and so does not vary as $\theta, \dot{\theta}$ are varied, hence a local minimum of S occurs when

$$\dot{\theta} = \pm \sqrt{\frac{2U}{M}}, \tag{44}$$

which implies $M\dot{\theta}^2 = 2U$. Solutions of this equation, which is equivalent to Eq. (33) with $c = V_0$, satisfy Eqs. (29) and (31) with the property that $S < \infty$. Hence, for such solutions we have $\dot{\theta} \to 0$ and θ approaches a zero of U as $|\tau| \to \infty$. We therefore integrate Eq. (44) or equivalently Eq. (33) with $c = V_0$.

For the first example we select a, b in the red region in Fig. 2 for which $1 < a < 2b-1$, with $c = V_0$ given by Eq. (41), then the soliton interpolates between the unstable steady states Eq. (24). By direct integration of Eqs. (33) or (44) we obtain

$$\cos\theta = 1 + \frac{2\kappa}{1 - (\kappa+1)\cosh^2 \sqrt{\kappa}(\tau - \tau_0)}, \tag{45}$$

where τ_0 is the constant of integration, and

$$\kappa = \frac{(a-1)(-a+2b-1)}{2(b-1)}.$$

The solution satisfies $\lim_{|\tau|\to\infty} \cos\theta = 1$ and at $\tau = \tau_0$, which may be regarded as the location of the soliton, we have $\cos\theta = -1$. By suitable choice of sign for θ, and by choice of the branch of the inverse cosine function, we obtain θ as a function of τ which either increases or decreases between any two adjacent zeros of the potential U at $\cos\theta = 1$. From Eq. (28) we obtain v:

$$v = \frac{a-1}{2(b-1)} + \frac{\kappa}{a - b \pm (b-1)\sqrt{\kappa+1}\cosh\sqrt{\kappa}(\tau - \tau_0)}, \tag{46}$$

where the sign corresponds to either increasing or decreasing θ, and we have $\lim_{|\tau|\to\infty} v(\tau) = \frac{a-1}{2(b-1)}$.

#165808 - $15.00 USD Received 30 Mar 2012; revised 27 May 2012; accepted 30 May 2012; published 14 Jun 2012

As a specific example, for $a = b = 2$ and $\kappa = 1/2$, the separatrix trajectory shown in Fig. 5(ii) is the parametric plot of v, θ as functions of the parameter τ; v evidently varies between maximum and minimum values which occur at $\tau = \tau_0$, as can be determined directly from Eq. (46). We can also find the solutions Eqs. (45) and (46) directly by solving Eq. (37). It is necessary only to determine $H_0 = H(v_0, \theta_0)$ by choosing v_0, θ_0 at $|\tau| = \infty$, which then determines Q from Eq. (38). For the states Eq. (24) we obtain $H_0 = -\frac{(a-1)^2}{4(b-1)}$ and $Q(v)$ has a repeated root at $v = \frac{a-1}{2(b-1)}$; the expression Eq. (46) for v may then be obtained by using the general integration formulas in Sections 2.266, 2.269 of Ref. [57].

Solitons also exist corresponding to the unstable steady states Eq. (25), provided $2b+1 < a < -1$ and $b < -1$, and may be obtained from the formulas Eqs. (45) and (46) by means of the symmetry $\tau \to -\tau, \theta \to \theta + \pi, a \to -a, b \to -b$ which leaves Eqs. (22) and (23) invariant. The parameter κ, for example, is now defined by $\kappa = (a+1)(a-2b-1)/2/(b+1)$ which is positive in the orange region of Fig. 2(ii).

Consider next the unstable states Eq. (26), which are defined only in the strip $|a| \leqslant 1$ of the a, b plane. Soliton solutions take the values $\cos\theta = a, v = 0$ as $|\tau| \to \infty$, and hence the Hamiltonian function $H(v, \theta)$ defined in Eq. (35) takes the constant value $H_0 = 0$, which corresponds to $c = V_0 = 2(a-b)$ in Eq. (33). By solving $\dot{v}^2 = Q(v)$ we find:

$$v(\tau) = \frac{1-a^2}{1-ab+|b-a|\cosh[\sqrt{1-a^2}\,(\tau-\tau_0)]}, \tag{47}$$

which exists for all $|a| < 1$ and $b \neq a$. We have $\lim_{|\tau|\to\infty} v(\tau) = 0$ and v attains its maximum value $v_{\max}$ at $\tau = \tau_0$, with either $v_{\max} = (a+1)/(b+1)$ for $b > a$ or else $v_{\max} = (a-1)/(b-1)$ for $b < a$. Having found v, we obtain $\cos\theta$ from Eq. (36) with $H_0 = 0$ using $\cos\theta = (a - bv)/(1-v)$, specifically

$$\cos\theta(\tau) = a - \frac{1-a^2}{-a+\eta\cosh[\sqrt{1-a^2}\,(\tau-\tau_0)]}, \tag{48}$$

where $\eta = (b-a)/|b-a|$ is the sign of $b-a$. We have $\dot{\theta} = a - \cos\theta$ and $\cos\theta(\tau_0) = -\eta$. For the special case $b = a$ with $|a| < 1$, or if $a = 1$, we solve $\dot{v}^2 = Q(v)$ directly; in the latter case we obtain

$$v(\tau) = \frac{2}{b+1+(b-1)(\tau-\tau_0)^2}, \qquad \cos\theta = 1 - \frac{2}{1+(\tau-\tau_0)^2}. \tag{49}$$

As a specific example we choose $a = 1, b = 4$, for which contour plots for constant H are shown in Fig. 5(i); the (red) separatrix trajectory in particular is visible as the curve which connects the unstable steady states at $v = 0, \theta = 0, 2\pi \ldots$. This separatrix is precisely the parametric plot of v, θ given by Eq. (49), where v evidently varies between zero and its maximum value of $2/(b+1) = 0.4$ which occurs at $\tau = \tau_0$, while $\cos\theta$ varies between the values 1 as $|\tau| \to \infty$, when $v = 0$, and -1 at $\tau = \tau_0$.

There are also solitons corresponding to the unstable steady states Eq. (27). Precise formulas can be obtained from Eqs. (47) and (48) by means of the transformations $\theta \to -\theta, v \to 1 - v, a \to -a + 2b$ which are discrete symmetries of the defining Eqs. (22) and (23).

Acknowledgments

This research was supported under the Australian Research Council's Discovery Project funding scheme (project number DP110104247). Tanya M. Monro acknowledges the support of an ARC Federation Fellowship.

#165808 - $15.00 USD Received 30 Mar 2012; revised 27 May 2012; accepted 30 May 2012; published 14 Jun 2012